analytical chemistry

Article

pubs.acs.org/ac

Sensitive Electrochemical Aptamer Biosensor for Dynamic Cell Surface *N*-Glycan Evaluation Featuring Multivalent Recognition and Signal Amplification on a Dendrimer−Graphene Electrode Interface

Xiaojiao Chen,[†,‡] Yangzhong Wang,[‡] Youyu Zhang,*[,†] Zhuhai Chen,[‡] Yang Liu,*[,‡] Zhaolong Li,[‡] and Jinghong Li[‡]

[†]Key Laboratory of Chemical Biology and Traditional Chinese Medicine Research (Ministry of Education), College of Chemistry and Chemical Engineering, Hunan Normal University, Changsha 410081, China

[‡]Beijing Key Laboratory for Analytical Methods and Instrumentation, Department of Chemistry, Tsinghua University, Beijing 100084, China

Supporting Information

ABSTRACT: We demonstrate a multivalent recognition and highly selective aptamer signal amplification strategy for electrochemical cytosensing and dynamic cell surface *N*-glycan expression evaluation by the combination of concanavalin A (Con A), a mannose binding protein, as a model, conjugated poly(amidoamine) dendrimer on a chemically reduced graphene oxide (rGO−DEN) interface, and aptamer- and horseradish peroxidase-modified gold nanoparticles (HRP−aptamer−AuNPs) as nanoprobes. In this strategy, the rGO−DEN can not only enhance the electron transfer ability but also provide a multivalent recognition interface for the conjugation of Con A that avoids the weak carbohydrate−protein interaction and dramatically improves the cell capture efficiency and the sensitivity of the biosensor for cell surface glycan. The high-affinity aptamer- and HRP-modified gold nanoparticles provide an ultrasensitive electrochemical probe with excellent specificity. As proof-of-concept, the detection of CCRF-CEM cell (human acute lymphoblastic leukemia) and its surface *N*-glycan was developed. It has demonstrated that the as-designed biosensor can be used for highly sensitive and selective cell detection and dynamic evaluation of cell surface *N*-glycan expression. A detection limit as low as 10 cells mL^{-1} was obtained with excellent selectivity. Moreover, this strategy was also successfully applied for *N*-glycan expression inhibitor screening. These results imply that this biosensor has potential in clinical diagnostic and drug screening applications and endows a feasibility tool for insight into the *N*-glycan function in biological processes and related diseases.

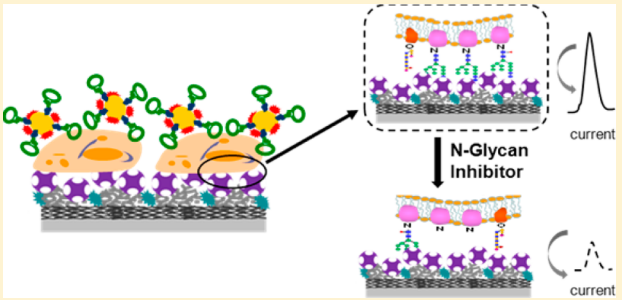

Cells are covered by a large number of glycans which are covalently attached to underlying proteins or lipids with high density and complex diversity.[1] The carbohydrate on the surface of a eukaryotic cell is in a complex milieu and plays vital roles in a broad range of crucial biological and physiological processes, including growth, development, differentiation, cell adhesion, cell−cell communication, signaling, immune response, disease, and progression of cancer.[2−7] Its expression is the subject of dynamic processes in which the cell surface characteristics undergo changes depending on the cellular condition and status. Glycan epitopes are used as useful surface markers to detect and recognize specific types of cells, such as tumor cells and stem cells, and reflect the pathophysiological steps of tumor progression.[8] For example, the binding of terminal high-mannose and mannose receptors on the cell surface is involved in the process of cellular fusion in osteoclast formation, and the aberrant expression of mannose is generally observed during the processes of tumorigenesis, brain aging, and differentiation.[9−11] As a result, dynamic analysis of cell surface glycans is primarily important to understand their roles in biological processes and clinical diagnostics.

A series of approaches, including high-performance liquid chromatography (HPLC),[12] mass spectrometry (MS),[13−15] nuclear magnetic resonance (NMR),[16] and capillary electrophoresis (CE),[17] have been developed for glycan analysis. Although these methods are powerful for detailed structure resolution, they are not suitable to the in situ glycan analysis of living cells due to their destructive procedures involving chemical labels or chemical and/or enzymatic release of the carbohydrates and are time-consuming with complicated sample preparation and sophisticated instrumentation. Recently, electrochemical carbohydrate biosensors based on the interaction of carbohydrates and lectins, a group of carbohydrate-specific binding proteins, have been developed in complementing the limitation of traditional methods for cell

Received: December 16, 2013
Accepted: March 31, 2014
Published: March 31, 2014

   dx.doi.org/10.1021/ac404070m | *Anal. Chem.* 2014, 86, 4278−4286

Scheme 1. (A) Schematic Illustration of the Electrochemical Aptamer Biosensor for Dynamic Evaluation of Cell Surface *N*-Glycan Expression Based on Multivalent Recognition and Dual Signal Amplification, (B) Fabrication of PAMAM Dendrimer-Conjugated Chemically Reduced Graphene Oxide (rGO−DEN), and (C) Fabrication Procedures of HRP- and Aptamer-Modified Au NP Nanoprobes (HRP−Aptamer−AuNPs)

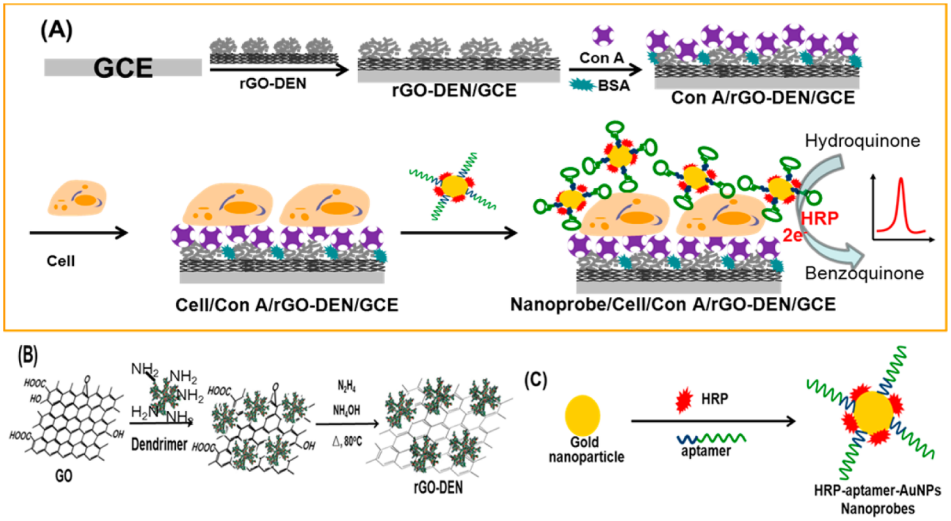

surface carbohydrate analysis due to their acceptable sensitivity, operational simplicity, flexibility, and low cost.[18−24] Various lectin-immobilized nanostrucuture electrode interfaces such as gold nanoparticles,[25] carbon nanotubes,[26,27] and conductive polymers[28] have been built for the highly sensitive detection of cells. In addition, multiple functional nanoprobes integrating specific carbohydrate recognition and enzymic catalysis were also developed for dynamic electrochemical monitoring of cell surface carbohydrates by coupling the nanostructure bio-interfaces.[3,9] However, the issues of active site accessibility and low affinity of the lectin and carbohydrate limit the sensitivity and stability of the biosensors.

Multivalent recognition is a general binding phenomenon in nature, especially for carbohydrate−protein interactions. Compared with the monovalent interaction, the multivalent system is proven to be an effective way to enhance the affinity by a factor as large as 10^4−10^5. Attempting to realize the maximized multivalency effects for proteins or cells has been rationally designed on the basis of numerous scaffolds such as dendrimers,[29] cyclodextrin,[30] and conducting polymers.[31] For example, poly(amidoamine) (PAMAM) dendrimers have been reported to be an excellent mediator for a facilitated multivalency effect owing to their capability to preorganize/orient ligands and the easy deformability of the polymer chains.[29,32] Dramatically increased cell capture efficiency was obtained on an antibody-conjugated dendrimer multivalent interface.[32] Recently, the multivalency effects were also observed by using nanoparticles as scaffolds such as gold nanoparticles and quantum dots for carbohydrates, antibodies, peptides, and DNA.[29,33−36] The large accommodation of the nanoparticle surface allows more active molecules to be loaded that enhance the recognition ratio. The "cluster effect" of the large scale of molecules can also improve the binding affinity. Moreover, the excellent photonic, electrochemical, and mechanical properties of nanoparticles allow them to be excellent transducers with extensive analytical techniques. Graphene, a two-dimensional carbon crystal with only one atom thickness, has drawn much attention because of its excellent electrical conductivity, high surface-to-volume ratio, remarkable chemical stability, easy functionalization, and excellent biocompatibility. The unique electric and photoelectrochemical characteristics of graphene have been broadly studied and applied in quantum electrical devices, electromechanical resonators, and electrochemical sensors.[24,37,38] Here, a PAMAM-conjugated graphene (rGO−DEN) composite electrode interface was developed by coupling the unique properties of graphene and PAMAM dendrimer, which can not only improve the electrode interface electron transfer but also enhance the multivalent recognition efficiency, and holds great promise in fabrication of biomimic devices and biosensors with high sensitivity.

Aptamers are artificially selected nucleic acid sequences with high affinity and specificity toward a wide range of small molecules, proteins, and cells.[39,40] In comparison to antibodies, aptamers possess a small size, a tunable structure, high resistance against denaturation, and programmable sequences which make them powerful affinity recognition ligands in clinical diagnostics. Recently, functional aptamers have been selected for targeting numerous cancers, and aptamer-conjugated nanomaterials have been extensively used for enhanced molecular recognition.[41−43] Due to the high affinity, excellent steric effect, and biocompatibility, aptamer nanomaterial conjugation is a brilliant prospect for the design of biosensor devices in drug delivery and clinical diagnostics.

In this work, a multivalent recognition and highly selective aptamer strategy for electrochemical cytosensing and dynamic cell surface *N*-glycan expression evaluation was designed by the combination of Concanavalin A (Con A), a mannose binding protein, as a model, conjugated PAMAM dendrimer on a chemically reduced graphene oxide (rGO−DEN) interface, and aptamer- and horseradish peroxidase-modified gold nanoparticles (HRP−aptamer−AuNPs) as nanoprobes (Scheme 1). To demonstrate the principle, a specific aptamer for CCRF-CEM cell (human acute lymphoblastic leukemia) capture was designed as a model. The abnormal glycan expression on the CCRF-CEM cell may be associated with fatal immune deficiency-associated diseases.[44] The dynamic and sensitive surface glycan monitoring of the CCRF-CEM cell provides a

dx.doi.org/10.1021/ac404070m | *Anal. Chem.* 2014, 86, 4278−4286

powerful tool for human immunodeficiency virus infection, drug screening, and the understanding of mechanisms of viral transmission at the molecular level.[45] In our strategy, rGO−DEN can not only enhance the electron transfer ability but also provide a multivalent recognition interface for the conjugation of Con A that avoids the weak carbohydrate−protein interaction and dramatically improves the cell capture efficiency and the sensitivity of the biosensor for cell surface glycan. Besides, the utilization of aptamer- and HRP-modified gold nanoparticles could increase the affinity between nanoprobes and cells and improve the selectivity of the biosensor. The experimental observations indicate that this strategy can not only recognize the cells with high specificity but also detect the cell and its surface glycan with high sensitivity. Moreover, this biosensor can be applied for dynamic monitoring of the expression of cell surface *N*-glycans, a particularly important class of carbohydrates accounting for about 90% of protein glycosylation that share a pentasaccharide core structure consisting of Manα1−6(Manα1−3)Manβ1−4GlcNAcβ1−4GlcNAc.[5,46,47] In addition, the strategy was investigated by the external stimuli of the *N*-glycan inhibitor tunicamycin (TM) or those released by peptide-*N*-glycosidase F (PNGase F). As expected, this biosensor is sensitive to *N*-glycan inhibitors and can be applied for *N*-glycan inhibitor screening. Therefore, the biosensor based on the multivalent interface and aptamer nanoprobes provides a valuable tool for the evaluation of cell surface *N*-glycan expression and opens new insight into the physiological functions of glycans in cellular processes as well as clinical diagnostics and drug screening.

EXPERIMENTAL SECTION

Reagents and Materials. Con A, fluorescein isothiocyanate-conjugated Con A (FITC−Con A), TM, and glutaraldehyde (GA) were purchased from Sigma-Aldrich. BG was obtained from Toronto Research Chemical Inc. (Canada). PNGase F was obtained from New England Biolabs Inc. (Ipswich, MA). Bovine serum albumin (BSA) and HRP (300 U mg^{-1}) were from Dingguo Biological Products Co. (Beijing, China). $HAuCl_4{\cdot}3H_2O$ (48%, w/w) was obtained from Shanghai Reagent (Shanghai, China). Graphite powder (99.99995%, 325 mesh) and tris(2-carboxyethyl)phosphine hydrochloride (TCEP) were purchased from Alfa Aesar. PAMAM (G3.0) dendrimer was purchased from Chenyuan Organosilicon New Material Co. (Weihai, China). The aptamer sequence was obtained from Shanghai Sangon Biological Engineering Technology & Services Co., Ltd. The sequence of the aptamer probe was as follows: 5′-SH-C_6H_{12}-TTT TTT TTT ATC TAA CTG CTG CGC CGC CGG GAA AAT ACT GTA CGG TTAGA-3′. Phosphate buffer solutions (PBS) were prepared with $Na_2HPO_4{\cdot}12H_2O$ and $NaH_2PO_4{\cdot}2H_2O$. The PBS (pH 7.4, 10 mM) containing 137 mM NaCl and 2.7 mM KCl was used as a washing solution, and the PBS (pH 7.0, 100 mM) containing 137 mM NaCl and 2.7 mM KCl was used as the electrolyte for detection. Other regents of analytical grade were obtained from Beijing Chemical Co. (China) and were used as received.

Synthesis of GO−DEN and rGO−DEN Conjugates. The graphene oxide (GO) was synthesized according to our previous works.[38] PAMAM-conjugated GO (GO−DEM) was prepared by the reaction of carboxyl groups on GO and amino groups on PAMAM to form a stable covalent interaction. Briefly, 2 mL of PAMAM dendrimer solution (50 μM) was added to 2 mL of GO solution (ca. 0.5 mg/mL) containing KOH (20 mM). The mixture was stirred at 40 °C for 12 h. A 160 μL volume of 0.5 M H_2SO_4 solution was then added, and the mixture was further stirred for 30 min. The resulting GO−DEN conjugates were collected, purified by centrifugation, and washed with deionized (DI) water several times. The GO−DEN was then chemically reduced by mixing 1 mL of the GO−DEN (ca. 0.3 mg/mL), 15 μL of hydrazine (35 wt % in DI water), and 11.8 μL of ammonia (25 wt % in DI water). Reduction occurred at 80 °C for 90 min to obtain the rGO−DEN conjugates.

Preparation of HRP−Aptamer−AuNP Nanoprobes. AuNPs were prepared by using citrate sodium as the reducing reagent. In brief, 100 mL of 0.01% (w/v) $HAuCl_4$ solution was boiled with vigorous stirring, and 2.5 mL of 1% (w/v) trisodium citrate solution was quickly added to the boiling solution. When the solution turned deep red, indicating the formation of AuNPs, the solution was left to stir and cool. The colloids were stored at 4 °C for further use.

Before conjugation, the thiolated aptamer (0.05 mM) was activated by 0.l mM TCEP in 50 mM Tris−HCl (pH 7.4) buffer for 1 h at room temperature, and 1 mL of 2-fold-concentrated AuNP colloidal solution was adjusted to pH 9.0 with 0.1 M K_2CO_3. Then 50 μL of HRP (1 mg/mL) was added, and the resulting solution was gently stirred at room temperature for 3 h. Subsequently, 14 μL of aptamer was added, and the solution was kept for another 24 h at 4 °C. After incubation, 100 μL of 1 M NaCl was added to the solution to "age" the aptamer, and the resulting solution was kept for another 24 h at 4 °C, followed by centrifugation for 15 min at 12 000 rpm. After the supernatant was discarded, the red pellets were washed twice with 10 mM PBS buffer (pH 7.4, containing 100 mM NaCl), and the resulting HRP−aptamer−AuNP conjugates were finally resuspended in PBS buffer and stored at 4 °C until use.

Cell Culture and Cell Treatment. CCRF-CEM cells were obtained from ATCC (American Type Culture Collection) and were cultured in RPMI 1640 medium (Dingguo Biological Products Co., Beijing, China) containing 10% fetal bovine serum (Dingguo), 100 U mL^{-1} penicillin, and 100 U mL^{-1} streptomycin at 37 °C in a humidified atmosphere of 5% CO_2. The cells at logarithmic growth were collected and separated from the medium by centrifugation at 800 rpm for 5 min and then washed with sterile Dulbecco's phosphate-buffered saline (DPBS, pH 7.4) twice. The sediment was resuspended in the DPBS to obtain a homogeneous cell suspension. The cell number was determined using a blood counting chamber. In the drug treatment assay, TM- and BG-treated CCRF-CEM cells were obtained by incubating 2×10^5 cells mL^{-1} in a culture medium containing 10 μg mL^{-1} (approximately 12 μM) TM and 550 μM BG for 48 h, respectively. PNGase F-treated CCRF-CEM cells were obtained by adding 3000 NEB units of PNGase F to the cell suspension with a concentration of 5×10^5 cells mL^{-1} for 24 h.

Biosensor Fabrication. The glassy carbon electrode (GCE; diameter of 3 mm) was pretreated by successively polishing with 0.3 and 0.05 μm α-Al_2O_3 powder followed by sonication in ethanol and distilled water, respectively. After being dried with a nitrogen flow, 6 μL of 1 mg mL^{-1} rGO−DEN solution was dropped onto the GCE, which was then dried overnight to obtain an rGO−DEN-modified electrode (rGO−DEN/GCE). Subsequently, the electrode was immersed in 100 μL of 2.5% GA solution for 1 h to activate amine groups on the film surface. Then 6 μL of 1 mg mL^{-1} Con A solution

dx.doi.org/10.1021/ac404070m | Anal. Chem. 2014, 86, 4278−4286

was dropped onto the film, which was then incubated for 1 h. Subsequently, the washed electrode was immersed in 1% BSA (w/v) solution for 1 h to block the nonspecific binding sites. Following a rinse with buffer, the Con A- and BSA-modified electrode (Con A/rGO−DEN/GCE) was soaked in 200 μL of CCRF-CEM cell suspension at a certain concentration containing 1 mM Ca^{2+} and Mn^{2+} and was incubated at 37 °C for 1 h to capture the cells via the specific binding between Con A and cell surface mannose and trimannoside. After being rinsed with PBS, the cell/Con A/rGO−DEN/GCE was obtained and used for subsequent differential pulse voltammetry (DPV) measurements.

Cell Surface *N*-Glycan Measurements. The cell/Con A/rGO−DEN/GCE was incubated with 30 μL of the HRP−aptamer−AuNP nanoprobe for 1 h at 37 °C. After being rinsed using PBS, the prepared HRP−aptamer−AuNP/cell/Con A/rGO−DEN/GCE was immersed in 2 mL of PBS (pH 7.0, 100 mM) solution with 3 mM hydroquinone (HQ) and 1.5 mM H_2O_2 and reacted for 6 min. The DPV measurements were performed from −0.3 to +0.2 V using a Ag/AgCl electrode with saturated KCl solution and platinum wire as the reference electrode and counter electrode, respectively.

Confocal Microscopy Imaging. CCRF-CEM cell (1×10^5 cells mL^{-1}) suspension was mixed with 10 μL of 1 mg mL^{-1} FITC−Con A containing 1 mM Ca^{2+} and 1 mM Mn^{2+}, and the resulting solution was incubated at room temperature for 30 min. The cells were collected by centrifugation at 1000 rpm for 5 min, following by washing twice with DPBS. Then the cell segments were resuspended in DPBS and assayed by confocal microscopy.

Apparatus and Characterization. Transmission electron microscopy (TEM) images were collected from a Hitachi H-7650B (Japan) at an accelerating voltage of 100 kV. The UV−vis spectra were obtained by a Hitachi U-3900 UV−vis spectrophotometer (Japan). Fourier transform infrared (FT-IR) spectra were recorded on a PerkinElmer Spectrum GX spectrometer (PerkinElmer Co., Waltham, MA). The X-ray diffraction (XRD) patterns were obtained using a D8 Advance (Bruker) X-ray diffractometer with Cu Kα radiation (λ = 1.5418 Å). An RM 2000 microscopic confocal Raman spectrometer (Renishaw PLC, England) with a 633 nm He−Ne laser beam was used for Raman spectrum collection. Confocal microscopy images were obtained on a Leica TCS SP5 microscope (Germany) with excitation at 488 nm.

Cyclic voltammetry (CV) and DPV were conducted on a CHI 440b instrument (CH Instruments, Inc., Austin, TX). Electrochemical impedance spectroscopy (EIS) was performed on a PARSTAT 2273 potentiostat/galvanostat (Advanced Measurement Technology Inc., Berwyn, PA) by applying an ac voltage of 5 mV amplitude with frequency from 0.01 to 10^5 Hz in 0.5 M KCl solution with 5 mM $K_3[Fe(CN)_6]$/$K_4[Fe(CN)_6]$ as the redox probe.

RESULTS AND DISCUSSION

Multivalent Recognition and Highly Selective Aptamer Signal Amplification Strategy. Scheme 1 presents the electrochemical aptamer biosensor for cytosensing and evaluating cell surface *N*-glycan expression based on multivalent recognition and dual signal amplification. The PAMAM dendrimer-conjugated rGO was first prepared and coated onto the surface of the GCE, which can not only promote the interface electron transfer rate but also supply a number of surface functional groups to accommodate multiple capture probes of Con A, thus enabling multivalent binding. The dendrimer-mediated multivalent binding between Con A and mannose or trimannoside, the core oligosaccharide of *N*-glycan on the cell surface, could improve the cell capture efficiency and thus enhance the sensitivity of the biosensor. After cells were captured, the electrode was incubated with the previously prepared electrochemical nanoprobe of HRP−aptamer−AuNPs to form a sandwich-type system based on the specific recognition between the aptamer and cell with high affinity, achieving higher selectivity and sensitivity of recognizing the cell as well as the surface glycan. Meanwhile, HRP−aptamer−AuNPs exploit the amplification effect of AuNPs for loading a large number of aptamers and HRP and enhancing the electrochemical catalysis signal of hydroquinone.[48] As a result, the sensitivity of the biosensor is greatly enhanced for cytosensing and cell surface *N*-glycan expression profiling.

Dendrimer-Conjugated rGO and HRP−Aptamer−AuNP Nanoprobe. The rGO−DEN was prepared by the covalent reaction between the amino groups in PAMAM dendrimer and the carboxyl groups in GO, followed by chemical reduction with hydrazine. The formation of rGO by the chemical reduction was confirmed by Raman spectra (Figure S1, Supporting Information). Figure 1A shows the FT-IR spectra of the chemically reduced graphene oxide (curve a), PAMAM dendrimer (curve b), and PAMAM-conjugated rGO (curve c). The IR spectrum of rGO shows a peak at 1626 cm^{-1} from the C═C stretching vibration of the aromatic ring in graphene (curve a). The peaks at 1553 and 1641 cm^{-1} in curve b correspond to the N−H bending vibration of amide II and C═O stretching vibration of amide I in PAMAM, respectively.[49] Curve c in Figure 1A presents the FT-IR spectrum of the as-prepared dendrimer-conjugated rGO. After PAMAM coupling, the peaks in curve c ascribed to the N−H bending vibration of amide II and C═O stretching vibration of amide I can also be observed except that they shift to 1559 and 1634 cm^{-1}, respectively. This fact confirms that PAMAM dendrimers are conjugated onto the rGO. Additionally, the successful conjugation was also confirmed by TEM as shown in Figure 1B. Like the graphenes reported, the PAMAM-conjugated rGO was nearly transparent flakelike and rippled and resembled crumpled silk veil waves, indicating that the covalent reaction does not change the structure of rGO.

Figure 1C presents the UV−vis spectra and TEM pattern (inset) of the gold nanoparticles (curve a) and HRP- and aptamer-modified gold nanoparticles (curve b). A strong adsorption at 520 nm was observed for the bare gold nanoparticles. After the conjugation of HRP and aptamer, the characteristic absorption peak of gold nanoparticles red shifted from 520 to 525 nm due to the decoration of biomolecules on the Au nanoparticles. Statistical analysis of the TEM data (inset) revealed that the average diameter of the gold nanoparticles was about 20 nm. These results demonstrate the accomplishment of the HRP−aptamer−AuNP nanoprobes.

Electrochemical Characterizations of the Biosensor. CV and EIS were used to verify the assembly processes of the modified electrodes step by step. Figure 2A displays the CV curves of the modified GCE using $Fe(CN)_6^{4-/3-}$ as an electroactive probe. A couple of reversible redox peaks for the bare GCE were observed in curve a. After the modification of dendrimer-conjugated rGO, the peak currents of the electrode increased (curve b). The increasing response is attributed to the large surface and the excellent electrical conductivity of dendrimer-conjugated rGO. When Con A was

dx.doi.org/10.1021/ac404070m | Anal. Chem. 2014, 86, 4278−4286

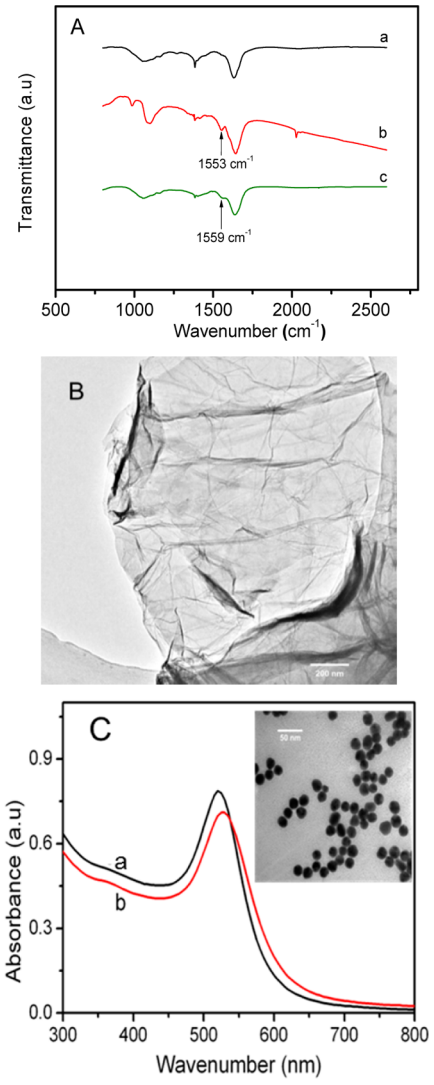

Figure 1. (A) FT-IR spectra of the chemically reduced graphene oxide (curve a), PAMAM dendrimer (curve b), and PAMAM-conjugated rGO (curve c). (B) TEM pattern of the PAMAM-conjugated rGO. (C) UV–vis spectra of the bare gold nanoparticles (a) and HRP- and aptamer-modified gold nanoparticles (b). The inset exhibits the TEM picture of the HRP–aptamer–AuNP nanoprobes.

immobilized onto the above electrode, the peak current decreased obviously and the peak gap of the redox potential became wider (curve c) owing to the electronically inert character of Con A. The peak currents in CV were further decreased, and the gap between the anodic and cathodic peaks became wider after subsequent capture of cells by the specific binding between Con A and cell surface mannose (curve d). This phenomenon results from the electronically inert feature of Con A and cell that block the electron transfer and mass transfer of $Fe(CN)_6^{4-/3-}$ ions at the modified GCE surface. Finally, the biosensor was incubated with the nanoprobe of HRP–aptamer–AuNPs. Although the gold nanoparticles generally show excellent conductivity and catalytic ability, the nanoprobe of HRP- and aptamer-loaded gold nanoparticles further blocks the electron transfer on the electrode interface, and a slight decrease in the peak currents was also observed (curve e).

The impedance spectra are shown in Figure 2B. The Nyquist plot comprises a semicircular part at higher frequency range

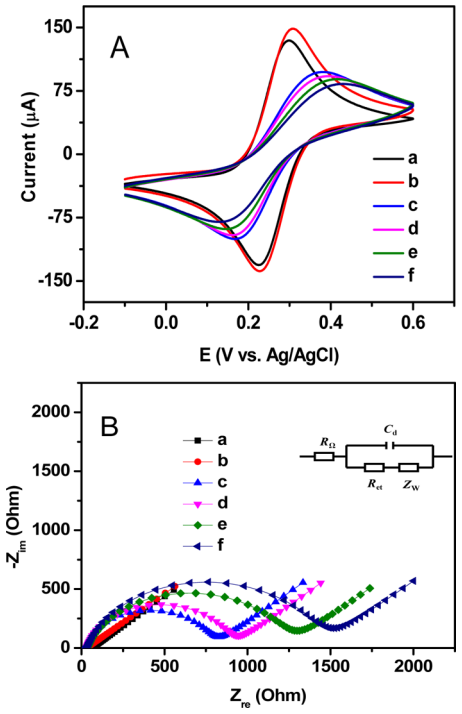

Figure 2. Cyclic voltammograms (A) and electrochemical impedance spectra (B) of (a) bare GCE, (b) rGO–DEN/GCE, (c) Con A/rGO–DEN/GCE, (d) BSA/ConA/rGO–DEN/GCE, (e) CCRF-CEM cell/BSA/ConA/rGO–DEN/GCE, and (f) HRP–aptamer–AuNPs/CCRF-CEM cell/BSA/ConA/rGO–DEN/GCE in 0.5 M KCl solution with 5 mM $[Fe(CN)_6]^{4-/3-}$ (scan rate 100 mV/s, impedance spectral frequency $0.1–10^5$ Hz, amplitude 10 mV). Inset: equivalent circuit of faradic electrochemical impedance (R_{es} = electrolyte resistance, C_d = double layer capacitance, R_{et} = electron transfer resistance, and Z_w = Warburg impedance).

and a straight linear part at lower frequency range. The diameter of the semicircle equals the electron transfer resistance (R_{et}) at the electrode interface. Due to the good electronic transfer ability, the dendrimer-conjugated rGO-modified GCE (curve b) exhibited lower R_{et} than bare GCE (curve a). After that the diameter of the semicircles increased successively with sequential assembly of Con A (curve c), cells (curve d), and HRP–aptamer–AuNP nanoprobes (curve e), showing the step-by-step increase of R_{et}. These results are consistent with those of CV, confirming the successful assembly of the biosensor.

Differential Pulse Voltammetry Behaviors of the Biosensor. The electrochemical behaviors of the biosensor were studied in 0.1 M PBS (pH 7.4) containing 1.5 mM H_2O_2 and 3 mM HQ. Figure 3A shows the DPV curves of the biosensors. A weak DPV peak current at ca. −0.05 V was observed (curve a) when the Con A/rGO–DEN/GCE was merely immersed in the electrolyte. The peak current increased after incubation of the Con A/rGO–DEN/GCE in the solution containing HRP–aptamer–AuNP nanoprobes (curve b). It is known that HRP is a mannose-containing glycoprotein with enzymatic activity. As a result, a small amount of HRP–aptamer–AuNP nanoprobes can be absorbed on the Con A-modified electrode based on the affinity interaction between Con A and the mannose groups in the nanoprobes. When the Con A/rGO–DEN/GCE was immersed in the solution with CCRF-CEM cells and subsequently in the solution of HRP–aptamer–AuNP nanoprobes, the DPV peak current increased

dx.doi.org/10.1021/ac404070m | Anal. Chem. 2014, 86, 4278–4286

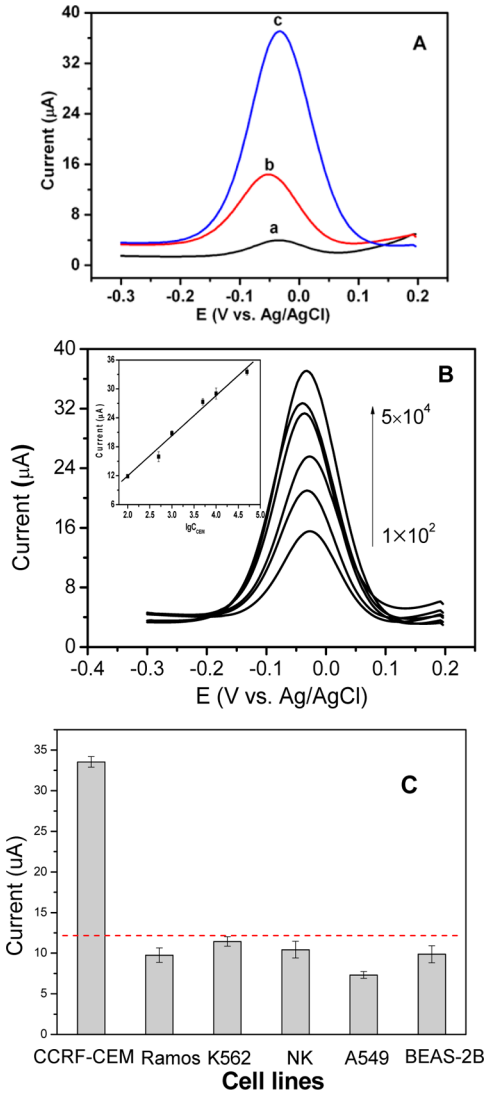

Figure 3. (A) Differential pulse voltammetry curves of the Con A/rGO−DEN/GCE (a), the electrode after incubation in HRP−aptamer−AuNP solution (b), and the electrode after incubation with CCRF-CEM cells and subsequently in HRP−aptamer−AuNP solution (c) in an electrolyte of 0.1 M PBS containing 1.5 mM H_2O_2 and 3 mM HQ. (B) DPV curves of the PAMAM-conjugated rGO-modified electrode in the solutions with CCRF-CEM cells at different concentrations of 1.0×10^2, 5.0×10^2, 1.0×10^3, 5.0×10^3, 1.0×10^4, and 5.0×10^4cells mL^{-1}. The electrolyte is 0.1 M PBS (pH 7.0) containing 3 mM HQ and 1.5 mM H_2O_2. The inset is a plot of the peak current intensity vs the logarithm value of the CCRF-CEM cell concentration. The error bars were obtained from three parallel experiments. (C) Peak current response of the electrochemical biosensor from the solution with different cell lines at a concentration of 5.0×10^4 cells mL^{-1}.

sharply (curve c), which was ascribed to not only the high affinity between mannose groups on the CCRF-CEM cell surface and Con A but also the highly specific interaction between the aptamer and CCRF-CEM cells. To verify the signal amplification effect of the nanoprobes, the DPV experiments were also conducted by immersing the CCRF-CEM cell/Con A/rGO−DEN/GCE in PBS with 3 mM HQ only. A very small peak current was presented (Figure S2, Supporting Information). It demonstrates that the DPV current originated from the electrocatalytic effect of HRP. Moreover, more HRP molecules loaded onto gold nanoparticles can further amplify the current signal; thus, the as-prepared biosensor is sensitive and feasible.

Optimization of the Experimental Conditions. The incubation time for nanoprobe adsorption is an important parameter for target cell capture and the specific recognition of the aptamer and cells. The dependence of the incubation time for HRP−aptamer−AuNP nanoprobes on the current response of the biosensor was studied and optimized as shown in Figure S3A (Supporting Information). When the CCRF-CEM cell-modified electrode was dipped into the solution with nanoprobes, the current signal increased with an incubation time of 1 h and reached a steady value even if a longer time was applied. Therefore, the optimal conditions of the biosensor were 60 min for cell capture and 60 min for nanoprobe incubation.

The current responses of the biosensor are significantly influenced by the pH and the concentration of HQ, which is the substrate of the enzymic catalytic reaction. Figure S3B (Supporting Information) shows the current signal as dependent on the pH of the electrolyte. It was observed that the current increased when the pH increased from 6.5 to 7.0 and then decreased when the pH was further increased to 8.5. As a result, a pH of 7.0 was selected for the amperometric detection. The current response to the concentration of HQ was also investigated as shown in Figure S3C. The current signal showed an intense increase when the concentration of HQ increased to 3 mM, and after that it exhibited a slow increase and reached a plateau. To minimize the damage of the cells on the electrode, an HQ concentration of 3 mM was used in the following experiments.

Cytosensing and Sensitivity of the Biosensor. On the basis of the optimal conditions, the determination of CCRF-CEM cells was applied using the multivalent recognition electrochemical biosensor. Figure 3B displays the DPV curves of the biosensor in the presence of CCRF-CEM cells with different concentrations. The peak current increased with increased concentration of the cells and was proportional to the logarithmic value of the cell concentration ranging from 1.0×10^2 to 5.0×10^4 cells mL^{-1}. The linear regression equation is $I = 8.33 \log[C_{cell}\ (\text{cells mL}^{-1})] - 4.68$ with a correlation coefficient of $R = 0.996$ ($n = 3$), where I is the peak current intensity and C_{cell} is the CCRF-CEM cell concentration. The detection limit for cell concentration was calculated to be 10 cells mL^{-1} at 3σ. It is obvious that the sensitivity of the multivalent recognition and dual signal amplification strategy is much higher than that of cancer cell cytosensors using Con A as the capture or recognition element reported in the literature (Table 1). The as-prepared biosensor displays excellent performance compared to some earlier reported methods, especially in the detection limit. The electrochemical cytosensor is based on the covalent attachment of PAMAM to the rGO adsorbed at the surface of the GC electrode. Higher numbers of functional groups on the rGO-modified electrode mediated by PAMAM afford a multivalent binding effect that significantly enhances the cancer cell capture efficiency and the surface binding strength of the tumor cells. Moreover, unlike those carbohydrate biosensors merely based on the lectin−carbohydrate interaction, the high affinity between the aptamer and cells also improves both the binding efficiency and the selectivity between the nanoprobes and thus enhances both the sensitivity and the selectivity of the biosensor. The biosensor was incubated with different cell lines such as CCRF-CEM

dx.doi.org/10.1021/ac404070m | Anal. Chem. 2014, 86, 4278−4286

Table 1. Comparison of Different Lectin-Based Electrochemical Biosensors for Cell Determination

detection method	cell line	linear range (cells mL^{-1})	detection limit (cells mL^{-1})	ref
cyclic voltammetry	HL-60	1.0×10^3 to 1.0×10^6	660	54
differential pulse voltammetry	Hela	8.0×10^2 to 2.0×10^7	500	21
stripping voltammetry	K562	1.0×10^2 to 1.0×10^7	100	55
stripping voltammetry	CCRF-CEM	1.0×10^2 to 1.0×10^5	50	24
photoelectrochemistry	SMMC-7721	5.0×10^3 to 1.0×10^7	5.0×10^3	56
electrochemiluminescence	BGC	2×10^3 to 1×10^7	1.2×10^3	25
electrochemiluminescence	K562	1.0×10^3 to 1.0×10^7	600	27
differential pulse voltammetry	CCRF-CEM	1.0×10^2 to 5.0×10^4	10	this work

(human acute lymphoblastic leukemia), Ramos (human Burkitt's lymphoma cell line), K562 (human immortalized myelogenous leukemia), NK (T cell, cytotoxic lymphocyte), A549 (human alveolar basal epithelial cells), and BEAS-2B (human bronchial epithelial cell), and the peak current response is shown in Figure 3C. A minimal current change was observed except that for CCRF-CEM cells even though the Ramos and K562 cells also belong to the leukemia cell line, showing the excellent selectivity of this biosensor and that it is promising in cancer cell detection and studies of the histopathological lesion process.

The reproducibility of the electrochemical aptamer biosensor was investigated by measuring the current signals with the cell concentration three times. The biosensor showed a relative standard deviation of 2.5% examined for three determinations at cell concentrations of 1×10^3 cells mL^{-1}, indicating good reproducibility of the biosensor. Thus, the as-proposed biosensor exhibits good performance in detecting cancer cell with a broad detection range, a low detection limit, and reproducibility and is promising for cancer cell detection and carbohydrate expression evaluation of living cells.

Evaluating Cell Surface *N*-Glycan Expression. The high sensitivity and facility of the proposed biosensor allows it to be further employed for evaluating the dynamic alteration of cell surface carbohydrate expression under external stimuli. TM and BG are the primarily inhibitors of cell surface *N*-glycan and *O*-glycan expression, respectively. The expression of cell surface carbohydrate was evaluated on the basis of Con A and dynamically under the treatment of tunicamycin (TM) and benzyl 2-acetamido-2-deoxy-α-D-galactopyranoside (BG) for a continuous 48 h (Figure 4A). Collating the TM-treated cells with untreated cells, a progressively decreasing current intensity can be observed. The current signal change was 39.6% after 48 h of treatment. The decreased current response of cell surface *N*-glycan expression was caused by TM, which could block the first step in the biosynthesis of N-glycosylation in cells for inhibiting *N*-glycans.[5,37] Confocal scanning microscopy was also applied to validate the *N*-glycan expression changes by treating CCRF-CEM cells in the stain with FITC-conjugated Con A (Figure S4, Supporting Information). After the treatment with TM for 48 h, the cells exhibited weaker fluorescence intensity than those without treatment, and the change in fluorescence intensity was calculated to be 35.2%, which confirms the observed change. It is noted that the electrochemical strategy offers a more direct and sensitive profile of glycans than confocal scanning microscopy, which could be attributed to the multivalent recognition effect on the electrode interface and the high affinity of the aptamer and cells as well as the dual signal amplification.

In addition, the treatment with BG, an *O*-glycan expression inhibitor but not an *N*-glycan inhibitor, was also studied. Nearly

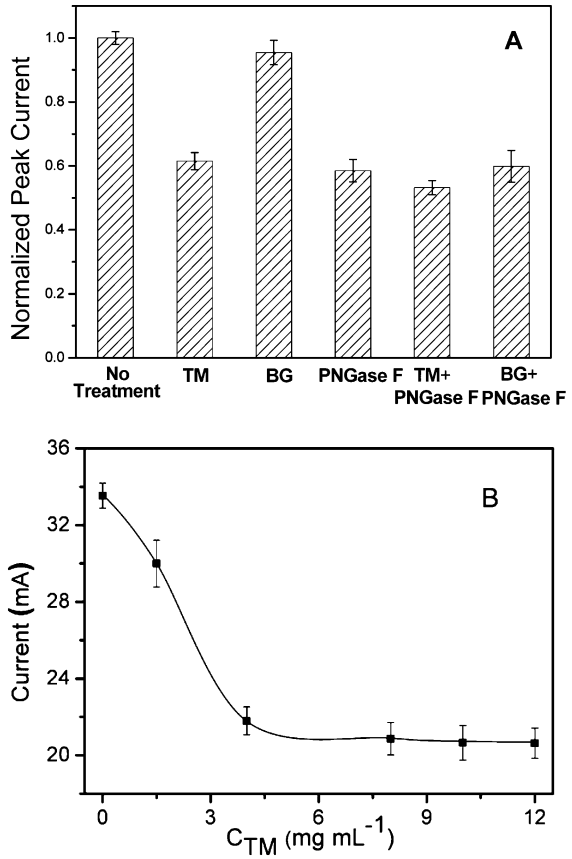

Figure 4. (A) *N*-Glycan expression of the CCRF-CEM cell surface without or with treatment with PNGase F and after incubation with TM (8 μg mL^{-1}) and BG (156 μg mL^{-1}). The electrolyte is 0.1 M PBS (pH 7.0) containing 3 mM HQ and 1.5 mM H_2O_2. The cell concentration is 5×10^4 cells mL^{-1}. (B) *N*-Glycan expression of the CCRF-CEM cell surface after incubation with different concentrations of TM for 48 h. The CCRF-CEM cell concentration is 5.0×10^4 cells mL^{-1}. The error bars were obtained from three parallel experiments.

no change was observed even though the concentration of BG (156 μg mL^{-1}) was much higher than that of TM (10 μg mL^{-1}, approximate 12 μM). The reason is that BG blocks the elaboration of the first-core GalNAc residues on O-linked glycoproteins for suppressing O-glycosylation but does not disturb N-glycosylation.[50,51] The electrochemical responses toward the different inhibition features between TM and BG validate the feasibility and reliability that a majority of the *N*-glycans on the cell surface could be recognized and evaluated by the as-designed carbohydrate biosensor.

Enzymatic cleavage and release of *N*-glycans from asparagine was performed by PNGase F, an amidase that cleaves between the innermost GlcNAc and asparagine residues of N-linked

dx.doi.org/10.1021/ac404070m | Anal. Chem. 2014, 86, 4278−4286

proteins.[5,52] The current intensity of PNGase F-treated cells was sharply dropped to 58.5% compared with that of untreated cells and was at the same level after enzymatic digestion with the treatments with TM and BG. As a result, the proposed electrochemical biosensor is able to be applied for cell surface *N*-glycan evaluation. It is demonstrated that the constructed biosensor provides a highly sensitive method for dynamically evaluating cell surface *N*-glycan expression. In addition, the inhibition of cell surface *N*-glycan expression in the presence of small-molecule inhibitors was also investigated. In the inhibition assay, the cell surface *N*-glycan expression was evaluated using TM as a model at different concentrations, and the half-maximal inhibition value (IC_{50}) was calculated. Figure 4B presents the peak current intensity as a function of the concentration of TM. It is clear that the peak current intensity decreased with increasing concentrations of TM and gradually reached a steady value after a concentration of ca. 4 μg mL^{-1} TM. Using these results, the IC_{50} was obtained on the basis of the concentration of the half peak current intensity from the steady current to the maximal peak current in the absence of inhibitor and was calculated to be 2.2 μg mL^{-1}, which was similar to that reported with a conventional assay.[53] Therefore, the as-designed biosensing strategy also affords a valuable tool that has potential in quantitatively screening small-molecule inhibitors for cell surface *N*-glycan expression.

CONCLUSION

In conclusion, a novel electrochemical cytosensor based on the multivalent recognition of Con A on the PAMAM-conjugated rGO electrode interface and mannose, especially the core trimannoside segment of *N*-glycan, was designed. By the integration of the high affinity between the aptamer and the cells as well as the signal amplification strategy, the as-designed biosensor can be used for highly sensitive cell detection and dynamic evaluation of cell surface *N*-glycan expression with a detection limit of 10 cells mL^{-1}. Moreover, the variations of *N*-glycans on the cell surface by the treatment of small-molecule inhibitors and enzymes were also sensed dynamically. The proof-of-concept method also shows excellent performance in the quantitative *N*-glycan inhibition assay, with verification with TM as a model. This strategy provides a highly sensitive method for dynamically analyzing changes of cell surface *N*-glycan in response to inhibitors and environmental stimulations. The novel strategy would contribute to the understanding of complex native glycan-related biological processes as well as serve as an impetus for elucidating the physiological processes of *N*-glycan-related diseases and clinical diagnostics.

ASSOCIATED CONTENT

Supporting Information

Additional information as noted in text. This material is available free of charge via the Internet at http://pubs.acs.org.

AUTHOR INFORMATION

Corresponding Authors

*Phone: 86-10-62798187. Fax: 86-10-62771149. E-mail: zhangyy@hunnu.edu.cn.

*E-mail: liu-yang@mail.tsinghua.edu.cn.

Notes

The authors declare no competing financial interest.

ACKNOWLEDGMENTS

This work was financially supported by the National Natural Science Foundation of China (Grants 21375073, 21005046, 21235004, and 21275051), the European Union Seventh Framework Programme (Grant 260600, GlycoHIT), and the Specialized Research Fund for the Doctoral Program of Higher Education (Grant 20100002120042).

REFERENCES

(1) Pilobello, K. T.; Mahal, L. K. *Curr. Opin. Chem. Biol.* **2007**, *11*, 300−305.
(2) Dennis, J. W.; Nabi, I. R.; Demetriou, M. *Cell* **2009**, *139*, 1229−1241.
(3) Haltiwanger, R. S.; Lowe, J. B. *Annu. Rev. Biochem.* **2004**, *73*, 491−537.
(4) Gu, J. G.; Isaji, T.; Xu, Q. S.; Kariya, Y.; Gu, W.; Fukuda, T.; Du, Y. G. *Glycoconjugate J.* **2012**, *29*, 599−607.
(5) Varki, A.; Cummings, R. D.; Esko, J. D.; Freeze, H. H.; Stanley, P.; Bertozzi, C. R.; Hart, G. W.; Etzler, M. E. *Essentials of glycobiology*, 2nd ed.; Cold Spring Harbor Press: Cold Spring Harbor, NY, 2009.
(6) Marth, J. D.; Grewal, P. K. *Nat. Rev. Immunol.* **2008**, *8*, 874−887.
(7) Lau, K. S.; Dennis, J. W. *Glycobiology* **2008**, *18*, 750−760.
(8) Fuster, M. M.; Esko, J. D. *Nat. Rev. Cancer* **2005**, *5*, 526−542.
(9) Zhang, X. A.; Teng, Y. Q.; Fu, Y.; Xu, L. L.; Zhang, S. P.; He, B.; Wang, C. G.; Zhang, W. *Anal. Chem.* **2010**, *82*, 9455−9460.
(10) Moremen, K. W.; Tiemeyer, M.; Nairn, A. V. *Nat. Rev. Mol. Cell Biol.* **2012**, *13*, 448−462.
(11) Morishima, S.; Morita, I.; Tokushima, T.; Kawashima, H.; Miyasaka, M.; Omura, K.; Murota, S. *J. Endocrinol.* **2003**, *176*, 285−292.
(12) Royle, L.; Campbell, M. P.; Radcliffe, C. M.; White, D. M.; Harvey, D. J.; Abrahams, J. L.; Kim, Y. G.; Henry, G. W.; Shadick, N. A.; Weinblatt, M. E.; Lee, D. M.; Rudd, P. M.; Dwek, R. A. *Anal. Biochem.* **2008**, *376*, 1−12.
(13) Kaneshiro, K.; Watanabe, M.; Terasawa, K.; Uchimura, H.; Fukuyama, Y.; Iwamoto, S.; Sato, T. A.; Shimizu, K.; Tsujimoto, G.; Tanaka, K. *Anal. Chem.* **2012**, *84*, 7146−7151.
(14) Liu, X.; McNally, D. J.; Nothaft, H.; Szymanski, C. M.; Brisson, J. R.; Li, J. J. *Anal. Chem.* **2006**, *78*, 6081−6087.
(15) Naka, R.; Kamoda, S.; Ishizuka, A.; Kinoshita, M.; Kakehi, K. *J. Proteome Res.* **2006**, *5*, 88−97.
(16) Bubb, W. A. *Concepts Magn. Reson., Part A* **2003**, *19A*, 1−19.
(17) Mechref, Y.; Novotny, M. V. *Mass Spectrom. Rev.* **2009**, *28*, 207−222.
(18) Chen, S. Y.; Zheng, T.; Shortreed, M. R.; Alexander, C.; Smith, L. M. *Anal. Chem.* **2007**, *79*, 5698−5702.
(19) Shen, Z. H.; Huang, M. C.; Xiao, C. D.; Zhang, Y.; Zeng, X. Q.; Wang, P. G. *Anal. Chem.* **2007**, *79*, 2312−2319.
(20) Cheng, W.; Ding, L.; Ding, S. J.; Yin, Y. B.; Ju, H. X. *Angew. Chem., Int. Ed.* **2009**, *48*, 6465−6468.
(21) Zhang, J. J.; Cheng, F. F.; Zheng, T. T.; Zhu, J. J. *Anal. Chem.* **2010**, *82*, 3547−3555.
(22) Lis, H.; Sharon, N. *Chem. Rev.* **1998**, *98*, 637−674.
(23) Cunningham, S.; Gerlach, J. Q.; Kane, M.; Joshi, L. *Analyst* **2010**, *135*, 2471−2480.
(24) Deng, J.; Liu, M.; Lin, F.; Zhang, Y.; Liu, Y.; Yao, S. *Anal. Chim. Acta* **2013**, *767*, 59−65.
(25) Han, E.; Ding, L.; Jin, S.; Ju, H. *Biosens. Bioelectron.* **2011**, *26*, 2500−2505.
(26) Liu, H.; Xu, S.; He, Z.; Deng, A.; Zhu, J.-J. *Anal. Chem.* **2013**, *85*, 3385−3392.
(27) Chen, Z.; Liu, Y.; Wang, Y.; Zhao, X.; Li, J. *Anal. Chem.* **2013**, *85*, 4431−4438.
(28) Wang, Z.; Sun, C.; Vegesna, G.; Liu, H.; Liu, Y.; Li, J.; Zeng, X. *Biosens. Bioelectron.* **2013**, *46*, 183−189.
(29) Gu, L.; Luo, P. G.; Wang, H.; Meziani, M. J.; Lin, Y.; Veca, L. M.; Cao, L.; Lu, F.; Wang, X.; Quinn, R. A.; Wang, W.; Zhang, P.; Lacher, S.; Sun, Y.-P. *Biomacromolecules* **2008**, *9*, 2408−2418.

(30) Vico, R. V.; Voskuhl, J.; Ravoo, B. J. *Langmuir* **2010**, *27*, 1391−1397.
(31) Ikeda, S.; Mori, Y.; Furuhashi, Y.; Masuda, H. *Solid State Ionics* **1999**, *121*, 329−333.
(32) Myung, J. H.; Gajjar, K. A.; Saric, J.; Eddington, D. T.; Hong, S. *Angew. Chem., Int. Ed.* **2011**, *50*, 11769−11772.
(33) Wang, Y. Z.; Chen, Z. H.; Liu, Y.; Li, J. H. *Nanoscale* **2013**, *5*, 7349−7355.
(34) de la Fuente, J. M.; Penadés, S. *Tetrahedron: Asymmetry* **2005**, *16*, 387−391.
(35) Earhart, C.; Jana, N. R.; Erathodiyil, N.; Ying, J. Y. *Langmuir* **2008**, *24*, 6215−6219.
(36) de la Fuente, J. M.; Barrientos, A. G.; Rojas, T. C.; Rojo, J.; Cañada, J.; Fernández, A.; Penadés, S. *Angew. Chem., Int. Ed.* **2001**, *40*, 2257−2261.
(37) Elbein, A. D. *Annu. Rev. Biochem.* **1987**, *56*, 497−534.
(38) Tang, L. H.; Wang, Y.; Li, Y. M.; Feng, H. B.; Lu, J.; Li, J. H. *Adv. Funct. Mater.* **2009**, *19*, 2782−2789.
(39) Tan, W.; Donovan, M. J.; Jiang, J. *Chem. Rev.* **2013**, *113*, 2842−2862.
(40) Li, D.; Song, S.; Fan, C. *Acc. Chem. Res.* **2010**, *43*, 631−641.
(41) Iliuk, A. B.; Hu, L.; Tao, W. A. *Anal. Chem.* **2011**, *83*, 4440−4452.
(42) Medley, C. D.; Bamrungsap, S.; Tan, W.; Smith, J. E. *Anal. Chem.* **2011**, *83*, 727−734.
(43) Sheng, W.; Chen, T.; Tan, W.; Fan, Z. H. *ACS Nano* **2013**, *7*, 7067−7076.
(44) Shangguan, D.; Li, Y.; Tang, Z.; Cao, Z. C.; Chen, H. W.; Mallikaratchy, P.; Sefah, K.; Yang, C. J.; Tan, W. *Proc. Natl. Acad. Sci. U.S.A.* **2006**, *103*, 11838−11843.
(45) Matsuoka, M.; Jeang, K. T. *Oncogene* **2011**, *30*, 1379−1389.
(46) Marino, K.; Bones, J.; Kattla, J. J.; Rudd, P. M. *Nat. Chem. Biol.* **2010**, *6*, 713−723.
(47) Nakano, M.; Saldanha, R.; Gobel, A.; Kavallaris, M.; Packer, N. H. *Mol. Cell. Proteomics* **2011**, *10*, 1−12.
(48) Liu, Y.; Liu, Y.; Feng, H.; Wu, Y.; Joshi, L.; Zeng, X.; Li, J. *Biosens. Bioelectron.* **2012**, *35*, 63−68.
(49) Popescu, M.-C.; Filip, D.; Vasile, C.; Cruz, C.; Rueff, J. M.; Marcos, M.; Serrano, J. L.; Singurel, G. *J. Phys. Chem. B* **2006**, *110*, 14198−14211.
(50) Dube, D. H.; Prescher, J. A.; Quang, C. N.; Bertozzi, C. R. *Proc. Natl. Acad. Sci. U.S.A.* **2006**, *103*, 4819−4824.
(51) Kuan, S. F.; Byrd, J. C.; Basbaum, C.; Kim, Y. S. *J. Biol. Chem.* **1989**, *264*, 19271−19277.
(52) Tretter, V.; Altmann, F.; Marz, L. *Eur. J. Biochem.* **1991**, *199*, 647−652.
(53) Matherly, L. H.; Angeles, S. M. *Biochem. Pharmacol.* **1994**, *47*, 1094−1098.
(54) Zheng, T.; Fu, J.-J.; Hu, L.; Qiu, F.; Hu, M.; Zhu, J.-J.; Hua, Z.-C.; Wang, H. *Anal. Chem.* **2013**, *85*, 5609−5616.
(55) Ding, L.; Cheng, W.; Wang, X.; Ding, S.; Ju, H. *J. Am. Chem. Soc.* **2008**, *130*, 7224−7225.
(56) Qian, Z.; Bai, H.-J.; Wang, G.-L.; Xu, J.-J.; Chen, H.-Y. *Biosens. Bioelectron.* **2010**, *25*, 2045−2050.